

Transmission spectra of the driven, dissipative Rabi model in the USC regime

L. Magazzù,¹ P. Forn-Díaz,^{2,3} and M. Grifoni¹

¹*Institute for Theoretical Physics, University of Regensburg, 93040 Regensburg, Germany*

²*Institut de Física d'Altes Energies (IFAE),*

The Barcelona Institute of Science and Technology (BIST), Bellaterra (Barcelona) 08193, Spain

³*Qilimanjaro Quantum Tech SL, Barcelona, Spain*

(Dated: May 1, 2022)

We present theoretical transmission spectra of a strongly driven, damped, flux qubit coupled to a dissipative resonator in the ultrastrong coupling regime. Such a qubit-oscillator system, described within a dissipative Rabi model, constitutes the building block of superconducting circuit QED platforms. The addition of a strong drive allows one to characterize the system properties and study novel phenomena, leading to a better understanding and control of the qubit-oscillator system. In this work, the calculated transmission of a weak probe field quantifies the response of the qubit, in frequency domain, under the influence of the quantized resonator and of the strong microwave drive. We find distinctive features of the entangled driven qubit-resonator spectrum, namely resonant features and avoided crossings, modified by the presence of the dissipative environment. The magnitude, positions, and broadening of these features are determined by the interplay among qubit-oscillator detuning, the strength of their coupling, the driving amplitude, and the interaction with the heat bath. This work establishes the theoretical basis for future experiments in the driven ultrastrong coupling regime and their impact to develop novel quantum technologies with superconducting circuits.

I. INTRODUCTION

Current developments in circuit quantum electrodynamics (QED) are establishing superconducting devices as leading platforms for quantum information and simulations [1–5]. In particular, quantum optics experiments with qubit coupled to superconducting resonators are now performed in (and beyond) the so-called ultrastrong coupling (USC) regime, with the qubit-resonator coupling reaching the same order of magnitude of the qubit splitting and resonator

frequency [6–16]. The strong entanglement between light and matter in the USC regime carries potential for designing novel quantum hybrid states and for achieving ultrafast information transfer [17]. In this parameter regime, the rotating-wave approximation, at the basis of the Jaynes-Cumming Hamiltonian, no longer applies as in typical quantum optics set-ups. The inclusion of counter-rotating terms in the light-matter coupling of a qubit with a cavity resonator leads to the so-called Rabi model theoretically investigated in this work.

In circuit QED platforms, the qubits are essentially based on superconducting circuits interrupted by Josephson junctions, the nonlinear elements that provide the anharmonicity required to single-out the two lowest energy states [18]. In the flux configuration [19], the qubit states are superpositions of clockwise and anti-clockwise circulating supercurrents, corresponding to the two lowest energy eigenstates of a double-well potential *seen* by the flux coordinate. The double-well can be biased by applying an external magnetic flux and transitions between states in this qubit basis, where the states are localized in the wells, occur via tunneling through the potential barrier of the potential.

The standard theoretical tool to account for the coupling of superconducting qubits to their electromagnetic or phononic environments is provided by the spin-boson model (SBM), consisting of a quantum two-level system interacting with a heat bath of harmonic oscillators [20, 21]. This model has been the subject of extensive studies as an archetype of dissipation in quantum mechanics and the different coupling regimes of spin-boson systems and the associated dynamical behaviors have been theoretically explored by using a variety of approaches [21, 22]. Only recently though, progress in the design of superconducting circuits has opened the possibility to attain experimental control on the strong qubit-environment coupling regime [23–28].

In circuit QED, an appropriate description for qubit-resonator systems is provided by the Rabi Hamiltonian, whose interaction part is featured by interaction terms known as counter-rotating. In this context, USC refers to an interaction regime where the rotating wave approximation, that allows for a description in terms of the Jaynes-Cummings Hamiltonian, appropriate for atom-cavity systems, fails, as the counter-rotating terms cannot be neglected [15, 16]. A refined classification of the different regimes of the Rabi model is provided in [29]. The USC regime of circuit QED is still the subject of much theoretical work, see for example [10, 11, 30–

33]. However, the intricacies of the driven Rabi problem in the USC regime [34] have been largely unexplored so far. Experiments on strongly driven qubits have demonstrated the possibility to control properties of engineered quantum two-level systems by intense light [25, 35, 36]. E.g. complex Landau-Zener patterns of avoided crossings could be controlled by tuning the driving amplitude, in agreement with theoretical expectations [5, 37, 38]. In recent works, spectroscopical signatures of drive-induced new symmetries [39] and nonadiabatic effects [40] in quantum systems have been addressed.

Experimentally, transmission spectroscopy has been shown to be a powerful tool to characterize the complex spectrum of the Rabi problem [9, 13, 14, 41]. Usually, the weak probe couples to the resonator, from which properties of the qubit can be inferred. As shown in this work, also a probe coupled to the qubit can provide precious information.

In this manuscript we consider a dissipative flux qubit ultrastrongly coupled to a superconducting resonator, modeled as a harmonic oscillator, which in turn interacts with a bosonic heat bath. The qubit is probed by a weak incoming field whose transmitted part provides information on the dynamics under the influence of the resonator and its environment, as demonstrated in a variety of experiments [42–46]. In addition, the qubit is subject to an intense microwave field, the drive. The setup considered describes quantum optics experiments in circuit QED but also the coupling of a qubit to a detector [47–49] and the qubit-bath coupling mediated by a waveguide resonator in a heat transport platform in the quantum regime [50]. Alternatives to the spectroscopy of the qubit to investigate USC systems exist. For example, spectroscopy of ancillary qubits has been proposed in [51] to probe the ground states of ultrastrongly-coupled systems. Moreover, methods alternative to the analysis of the transmission spectra have been recently devised to probe the USC regime [52, 53].

Weak dissipation affecting a USC system as a whole has been addressed via a master equation approach in [8, 54]. Since our USC system is probed through the qubit, here we conveniently map the dissipative Rabi model which describes our setup to an effective spin-boson model where the spin interacts directly with a bosonic bath characterized by an effective spectral density. The latter function is peaked at the oscillator frequency [55], and thus describes a so-called structured environment. Using the same approach as the one developed in [25, 56] to analyze the measured

transmission of a probe field in the presence of an Ohmic environment and of a pump drive, here we calculate the transmission spectra of the qubit, considering different qubit-resonator detuning and coupling strengths, as well as driving amplitudes. Specifically, the qubit's response function is evaluated within the so called non-interacting blip approximation (NIBA), which allows one to treat dissipation (and hence the effects of the resonator) as well as the strong drive in a non-perturbative way [37]. In absence of the drive, our results for the transmission spectra show clear signatures of the non trivial entanglement between qubit and cavity in the form of avoided crossings, whose amplitude depends on the qubit-resonator coupling strength. When the drive is added, the avoided crossing further reveal the entanglement of the qubit with *both* cavity photons and quanta of the driving field.

The paper is structured as follows. In Section II the driven and dissipative Rabi model and its mapping to an effective, driven spin boson model is discussed. In Sec. III spectral properties of the non-dissipative Rabi model in the USC regime are analyzed, while a formal expression for the transmission is shortly reported in Sec. IV. Numerical results are shown in Sec. V, and interpreted on the basis of the analytical results of Sec. III. Finally, conclusions are drawn in Sec. VI.

II. THE DRIVEN, DISSIPATIVE RABI MODEL

For a realistic description of experiments with USC systems, the inclusion of decoherence and dissipative effects induced by the electromagnetic environment or by other sources is unavoidable. Previous work used a modified master equation to include the effect of dissipation in the perturbative USC regime [57, 58]. In the following, we consider a driven, dissipative flux qubit coupled to a resonator which is in turn subject to dissipation. Specifically, qubit and resonator interact with two independent Ohmic heat baths, denoted by 1 and r, respectively. The qubit is characterized by the tunneling matrix element Δ , while the resonator is modeled as a harmonic oscillator of frequency Ω . These two systems are coupled with an interaction strength quantified by the frequency g . If g is of the order of Δ and Ω the system is in the ultrastrong coupling regime. The full Hamiltonian of this driven, dissipative Rabi model, which is sketched

in Fig. 1(a), is

$$\begin{aligned}
H(t) = & -\frac{\hbar}{2} [\Delta\sigma_x + \epsilon(t)\sigma_z] + \hbar\Omega B^\dagger B - \hbar\sigma_z g(B^\dagger + B) \\
& + \sum_{k=1}^{N_1} \hbar\omega_{1k} b_{1k}^\dagger b_{1k} + \sum_{k=1}^{N_r} \hbar\omega_{rk} b_{rk}^\dagger b_{rk} - \frac{\hbar}{2} \sigma_z \sum_{k=1}^{N_1} \lambda_{1k} (b_{1k}^\dagger + b_{1k}) - \hbar(B^\dagger + B) \sum_{k=1}^{N_r} \lambda_{rk} (b_{rk}^\dagger + b_{rk}) ,
\end{aligned} \tag{1}$$

where the qubit operators $\sigma_z = |\downarrow\rangle\langle\downarrow| - |\uparrow\rangle\langle\uparrow|$ and $\sigma_x = |\downarrow\rangle\langle\uparrow| + |\uparrow\rangle\langle\downarrow|$ are expressed in the so-called qubit basis of localized right- and left-well states $|\downarrow\rangle, |\uparrow\rangle$. The qubit is driven by the time-dependent bias

$$\epsilon(t) = \epsilon_0 + \epsilon_p \cos(\omega_p t) + \epsilon_d \cos(\omega_d t) , \tag{2}$$

which is the sum of a static part ϵ_0 , a weak probe (p), and a drive (d), with arbitrary amplitude, which we will assume to be of high frequency, see Fig. 1(c).

The bosonic creation and annihilation operators $B^\dagger, b_{1/rk}^\dagger$ and $B, b_{1/rk}$ create and destroy an excitation in the resonator and in the k -th harmonic oscillator of the qubit/resonator bath, respectively. The angular frequencies $\lambda_{1/rk}$ correspond to the coupling strengths with the individual modes of the baths. Note that, by removing the resonator and its bath from the full Hamiltonian (1), we are left with the standard spin-boson Hamiltonian [20]. On the other hand, removing the baths coupled to qubit and resonator, the standard Rabi Hamiltonian is recovered.

Each bath is fully characterized by the spectral density function

$$G(\omega) = \sum_k \lambda_k^2 \delta(\omega - \omega_k) . \tag{3}$$

In the continuum limit, we assume an Ohmic spectral density with exponential cutoff for the qubit, i.e. $G_1(\omega) = 2\alpha_1 \omega e^{-\omega/\omega_c}$, with ω_c a high-frequency cutoff, and a strictly Ohmic spectral density $G_r(\omega) = \kappa\omega$ for the resonator. The dimensionless dissipation strengths are related to the friction coefficient in the Caldeira-Leggett model [21, 59, 60], see Appendix A.

Figure 1(d) shows a schematic of the implementation of the driven, dissipative Rabi model using a superconducting circuit. A 3-junction flux qubit is galvanically attached to an LC resonator in order to attain ultrastrong coupling strengths, while keeping the interaction linear. In addition, two superconducting waveguides couple to the qubit and resonator, in order to define their own respective ohmic baths. The coupling to the baths determines the decay rate

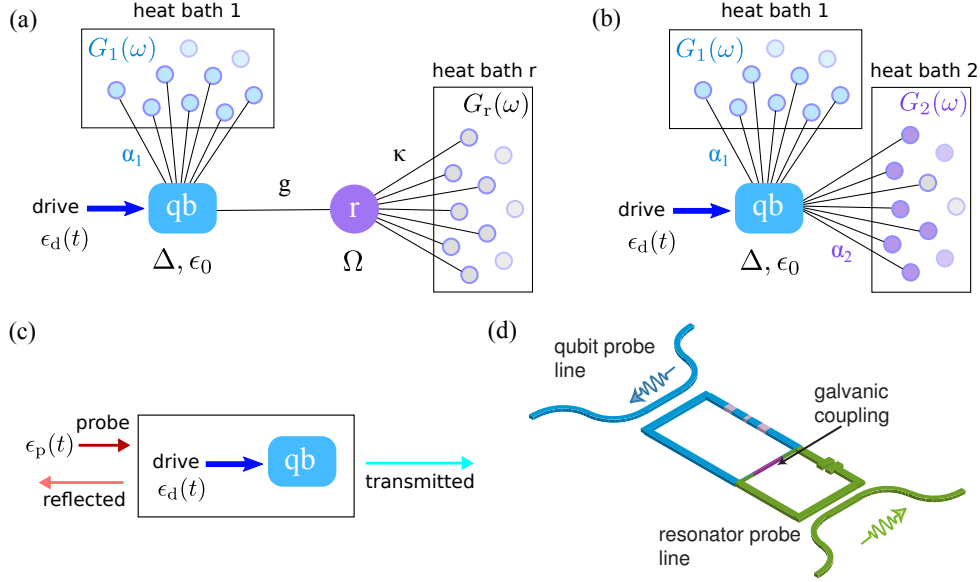


Fig. 1. Model and experimental design of the driven dissipative Rabi model. (a) The dissipative Rabi model is realized by coupling a flux qubit to an Ohmic heat bath, denoted with 1, and to a resonator, which is in turn coupled to an Ohmic environment, denoted with r. (b) The model is mapped into a two-bath spin-boson model, where the qubit is coupled to two heat baths. The first is the original bath 1 while the second, denoted by 2, is a structured effective bath. (c) Detail of the two-tone spectroscopy protocol where the transmission line is used to probe the driven qubit, the drive being applied via the transmission line as well. (d) Simplified circuit implementation of the USC system displaying the qubit (large loop interrupted by three Josephson junctions) and the LC resonator (smaller loop). The qubit and resonator are galvanically connected to enhance the coupling strength into the USC regime. The qubit/resonator probing lines correspond to their respective ohmic environments.

of each system, with an additional loss channel into intrinsic microscopic noise present in the neighborhood of the circuit.

The full Hamiltonian of the model, Eq. (1), can be mapped to that of the two-bath spin-boson model depicted in Fig. 1(b) which reads

$$H_{\text{SB}}(t) = -\frac{\hbar}{2} [\Delta \sigma_x + \epsilon(t) \sigma_z] - \frac{\hbar}{2} \sigma_z \sum_{\nu k} \lambda_{\nu k} (a_{\nu k}^\dagger + a_{\nu k}) + \sum_{\nu k} \hbar \omega_{\nu k} a_{\nu k}^\dagger a_{\nu k}. \quad (4)$$

In this effective Hamiltonian, the qubit is directly coupled to two bosonic baths indexed with $\nu = 1, 2$: the bath 1 is the same Ohmic bath coupled to the qubit as in Eq. (1). The second,

$\nu = 2$ is a new, *effective* bath whose spectral density, in the continuum limit, reads [48, 55, 61–63]

$$G_2(\omega) = \frac{2\alpha_2\omega\Omega^4}{(\Omega^2 - \omega^2)^2 + (\gamma\omega)^2} . \quad (5)$$

This effective spectral density is structured, meaning that it displays a peak centered at the oscillator frequency Ω with width $\gamma = 2\pi\kappa\Omega$. The latter frequency is the memoryless damping kernel of the resonator's Ohmic bath, see Appendix A. The corresponding effective coupling strength α_2 is given by the dimensionless parameter $\alpha_2 = 8\kappa g^2/\Omega^2$. In the limit $\Omega \ll \Delta$ the qubit sees a bath with a low-frequency Ohmic behavior. By taking the limit $\kappa \rightarrow 0$ (i.e. disconnecting the Ohmic bath interacting with the resonator), we obtain $\lim_{\kappa \rightarrow 0} G_2(\omega) = 4g^2\delta(\omega - \Omega)$, which consistently describes the bath $\nu = 2$ as comprising a single oscillator coupled to the qubit with strength $\lambda = 2g$. The resulting interaction term in Eq. (4) reproduces the qubit-resonator coupling term in Eq. (1). This problem displays high complexity due to the strong driving on the qubit, the ultrastrong coupling between qubit and resonator, as well as environmental effects on both qubit and oscillator. In order to gain physical insight, we first recall some features of the spectrum of the driven Rabi system in the absence of dissipation.

III. ANALYTICAL TREATMENT OF THE CLOSED RABI MODEL IN THE USC REGIME

A. Closed Rabi model in the USC regime

We start with the non-driven, non-dissipative Rabi model, whose spectrum has been discussed in various works by now, see e.g. [8, 10, 11, 64, 65]. Following the polaron approach, an approximate analytical expression for the spectrum of the Rabi model can be derived using Van Vleck perturbation theory in the qubit's tunneling parameter Δ . The approximation is nonperturbative in the qubit-resonator coupling strength g and performs excellently [11] for negative detuning ($\Omega > \Delta$).

For $\Delta = 0$, the eigenstates of the system are composed of tensor products of displaced oscillator and qubit eigenstates. The exact spectrum is given by the combination of qubit and

resonator energies

$$E_{\mp,j} = \mp \frac{\hbar}{2} \epsilon_0 + \hbar j \Omega - \hbar \frac{g^2}{\Omega}, \quad j = 0, 1, 2, \dots \quad (6)$$

A finite tunneling Δ mixes the eigenstates nontrivially. To find an approximate analytical solution, we notice that for static bias values $\epsilon_0 = l\Omega$ one can identify two-fold degenerate subspaces in the complete Hilbert space of the problem: $E_{+,j} = E_{-,l+j}$. A finite tunneling removes the degeneracy and induces coupling among the dressed states. Using Van Vleck perturbation theory to lowest order in the tunneling one finds the modified energies [11]

$$E_{\mp,j}^l \simeq \hbar \left[\left(j + \frac{l}{2} \right) \Omega - \frac{g^2}{\Omega} + \frac{1}{8} \left(\varepsilon_{\downarrow,j}^{(2),l} - \varepsilon_{\uparrow,j+l}^{(2),l} \right) \mp \frac{1}{2} \Omega_j^l \right]. \quad (7)$$

For the level splitting in Eq. (7) it is found

$$\Omega_j^l = \sqrt{\left[\epsilon_0 - l\Omega + \frac{1}{4} \left(\varepsilon_{\downarrow,j}^{(2),l} + \varepsilon_{\uparrow,j+l}^{(2),l} \right) \right]^2 + \left(\Delta_j^{j+l} \right)^2}, \quad (8)$$

where the so-called diagonal corrections are given by

$$\varepsilon_{\downarrow/\uparrow,j}^{(2),l} = \sum_{\substack{k=-j \\ k \neq \pm l}}^{\infty} \frac{\left(\Delta_j^{k+j} \right)^2}{\epsilon_0 \mp k\Omega}. \quad (9)$$

The dressed tunneling elements depend on the numbers j and j' of oscillator quanta involved in the dressing and read

$$\Delta_j^{j'} = \Delta [\text{sgn}(j' - j)]^{|j' - j|} D_{\min\{j,j'\}}^{|j' - j|}(\tilde{\alpha}), \quad (10)$$

with

$$D_j^k(\tilde{\alpha}) = \tilde{\alpha}^{k/2} \sqrt{\frac{j!}{(j+k)!}} \mathbb{L}_j^k(\tilde{\alpha}) e^{-\frac{\tilde{\alpha}}{2}}, \quad (11)$$

and $\tilde{\alpha} = (2g/\Omega)^2$. Here, $\mathbb{L}_j^k(\tilde{\alpha})$ are the generalized Laguerre polynomials defined by the recurrence relation

$$\mathbb{L}_{j+1}^k(\tilde{\alpha}) = \frac{(2j+1+k-\tilde{\alpha})\mathbb{L}_j^k(\tilde{\alpha}) - (j+k)\mathbb{L}_{j-1}^k(\tilde{\alpha})}{j+1}, \quad (12)$$

with $\mathbb{L}_0^k(\tilde{\alpha}) = 1$ and $\mathbb{L}_1^k(\tilde{\alpha}) = 1 + k - \tilde{\alpha}$. For $|\epsilon_0| < \Omega$ we fix $l = 0$.

For $\Omega = \epsilon_0$, corresponding to $l = 1$, one finds for the avoided crossing involving the first and

second excited state, $\Delta_0^1 = \Delta\sqrt{\tilde{\alpha}}e^{-\tilde{\alpha}/2}$. In the limit of small $\tilde{\alpha}$, one can expand the dressed tunneling splittings in order to obtain the famous Rabi splitting of the Jaynes-Cummings model which, at resonance, assumes the value $2\hbar g\sqrt{j+1}$. Noticeably, in the high-photon limit, $j, j' \rightarrow \infty$, and for finite $j - j'$, this dressing by Laguerre polynomials becomes a dressing by Bessel functions known for quantum systems in intense electromagnetic fields [37]. The interplay between quantum and classical radiation is the topic of the next subsection.

B. Driven Rabi model

We include now a drive on the qubit. The picture is enriched, with respect to the static case, by the presence of new resonances and by the modulation induced by the Bessel functions, which stems from the classical drive, on top of the Laguerre dressing given by the quantum oscillator, i.e. the resonator. The spectrum can now be calculated within a dressed Floquet picture, with quasi-energies known exactly for the case $\Delta = 0$. Similar to the static case, two-fold degeneracies now occur when $\epsilon_0 = l\Omega - m\omega_d$. Within leading order Floquet-Van Vleck perturbation theory in Δ , the quasi-energy spectrum of the driven, nondissipative Rabi model now reads ¹ [34]

$$E_{\mp, n, j}^{m, l} = \hbar \left[-\left(n + \frac{m}{2}\right) \omega_d + \left(j + \frac{l}{2}\right) \Omega - \frac{g^2}{\Omega} + \frac{1}{8} (\varepsilon_{\downarrow, n, j}^{(2), m, l} - \varepsilon_{\uparrow, n+m, j+l}^{(2), m, l}) \mp \frac{1}{2} \Omega_{n, j}^{m, l} \right], \quad (13)$$

where the n and j denote the Floquet mode and oscillator quantum number, respectively, while m and l give the resonance condition. The doublets' amplitudes are now given by, cf. Eq. (8),

$$\Omega_{n, j}^{m, l} = \sqrt{\left[\epsilon_0 + m\omega_d - l\Omega + \frac{1}{4} (\varepsilon_{\downarrow, n, j}^{(2), m, l} + \varepsilon_{\uparrow, n+m, j+l}^{(2), m, l}) \right]^2 + \left(\Delta_{n, j}^{m+n, j+l} \right)^2}, \quad (14)$$

where the diagonal corrections read

$$\varepsilon_{\downarrow/\uparrow, n, j}^{(2), m, l} = \sum_{\substack{p=-\infty \\ p \neq -m}}^{\infty} \sum_{\substack{k=-j \\ k \neq \pm l}}^{\infty} \frac{\left(\Delta_{n, j}^{n+p, k+j} \right)^2}{\epsilon_0 + p\omega_d \mp k\Omega}. \quad (15)$$

The tunneling elements are further dressed by Bessel functions as

$$\Delta_{n, j}^{n', j'} = J_{n'-n}(\epsilon_d/\omega_d) \Delta_j^{j'}, \quad (16)$$

¹ We keep the same convention for the indexes as in [11].

with $\Delta_j^{j'}$ defined in Eq. (10). Noticeably, the bare tunneling splitting is now dressed by *both* quanta of the resonator and of the driving microwave radiation.

At the symmetry point $\epsilon_0 = 0$ the resonances still occur when $m\omega_d = l\Omega$. For example, in the case $m = 1$, $l = 1$, one finds avoided crossings with tunneling splitting $\Delta_{n,j}^{n+1,j+1} = J_1(\epsilon_d/\omega_d)\Delta_j^{j+1}$.

As we shall see in the Sec. V, these resonances dominate the transmission spectra of the driven Rabi model. Before this, we illustrate in the coming section how to relate the qubit transmission spectra, namely the spectral properties of the Rabi model as probed in the experimental setup, see Fig. 1(c)-(d), to the steady-state response of the qubit.

IV. TRANSMISSION

In actual experiments, see Fig. 1(c), the probe field $V_{\text{in}}^{\text{p}}(t) = f_Z \epsilon_p \cos(\omega_p t)$ is applied to the qubit via an external transmission line. Following [25, 66], the corresponding transmitted field is $V_{\text{transm}}(t) = V_{\text{in}}^{\text{p}}(t) - f\dot{P}(t)/2$, where $P(t) := \langle \sigma_z(t) \rangle$ is the so-called qubit population difference in the localized qubit basis. The proportionality constants f_Z and f depend on the details of the experimental setup and have dimensions of a magnetic flux. In terms of the Fourier-transformed probe and transmitted fields calculated at the probe frequency, the transmission is defined as the square modulus of the complex coefficient

$$\mathcal{T}(\omega_p) = \tilde{V}_{\text{transm}}(\omega_p) / \tilde{V}_{\text{in}}^{\text{p}}(\omega_p) . \quad (17)$$

At the steady state, the population difference has the period of the probe, also in the presence of a high-frequency drive, provided that we average over its period $2\pi/\omega_d$ the kernels of the generalized master equation (GME) for $P(t)$, see Appendix B. Expanding in Fourier series the time-periodic asymptotic population difference $P_{\text{as}}(t) = \lim_{t \rightarrow \infty} P(t)$ as ²

$$\dot{P}_{\text{as}}(t) = \sum_m -im\omega_p p_m e^{-im\omega_p t} , \quad (18)$$

where

$$p_m = \frac{\omega_p}{2\pi} \int_{-\pi/\omega_p}^{\pi/\omega_p} dt P_{\text{as}}(t) e^{im\omega_p t} , \quad (19)$$

² Note the different convention used for the signs with respect to Ref. [25].

we find for the transmission at the probe frequency ω_p , within linear response to the probe field,

$$\mathcal{T}(\omega_p) = 1 + i\mathcal{N}\hbar\omega_p\chi(\omega_p), \quad (20)$$

where $\mathcal{N} = f/f_Z$ and $\chi(\omega_p) = p_1/\hbar\epsilon_p$. Within the non-interacting blip approximation (NIBA) [20, 21, 67], the GME that describes the driven, dissipative qubit dynamics, yields an analytical expression for the linear susceptibility $\chi(\omega_p)$, see Appendix C, which is nonperturbative in the qubit-baths coupling. It reads

$$\chi(\omega_p) = \frac{(\hbar\omega_p)^{-1}}{-i\omega_p + \hat{k}_0^+(-i\omega_p)} \left[\hat{\kappa}_{+1}^-(0) - \hat{\kappa}_{+1}^+(0) \frac{\hat{k}_0^-(0)}{\hat{k}_0^+(0)} \right], \quad (21)$$

where the GME kernels are defined as

$$\begin{aligned} \hat{k}_0^\pm(\lambda) &= \Delta^2 \int_0^\infty d\tau e^{-\lambda\tau} e^{-Q'(\tau)} c^\pm[Q''(\tau)] J_0 \left[\frac{2\epsilon_d}{\omega_d} \sin\left(\frac{\omega_d\tau}{2}\right) \right] c^\pm(\epsilon_0\tau), \\ \hat{\kappa}_1^\pm(0) &= \mp \Delta^2 \int_0^\infty d\tau e^{i\omega_p\tau/2} e^{-Q'(\tau)} c^\pm[Q''(\tau)] J_0 \left[\frac{2\epsilon_d}{\omega_d} \sin\left(\frac{\omega_d\tau}{2}\right) \right] \sin(\omega_p\tau/2) c^\mp(\epsilon_0\tau), \end{aligned} \quad (22)$$

with $c^+(x) = \cos(x)$ and $c^-(x) = \sin(x)$, see also [25, 37, 56]. Here, $J_0(x)$ is the Bessel function of the first kind [68], which stems from averaging the kernels over the drive period, see Appendix D.

The baths' correlation function is the sum $Q(t) = \sum_\nu Q_\nu(t)$, where

$$Q_\nu(t) = \sum_\nu \int_0^\infty d\omega \frac{G_\nu(\omega)}{\omega^2} \left[\coth\left(\frac{\hbar\omega\beta_\nu}{2}\right) (1 - \cos\omega t) + i \sin\omega t \right], \quad (23)$$

with $\beta_\nu := (k_B T_\nu)^{-1}$ the inverse temperature of bath ν . Explicit expressions for $Q_\nu(t)$ are provided in Appendix B. By inspection of Eqs. (20)-(22), we note that the transmission in linear response is independent of the probe amplitude ϵ_p .

Thus, the complex physics of the dissipative Rabi model is fully captured by the kernels in Eq. (22) together with the associated correlation functions, Eq. (23). Numerical results for the transmission and their interpretation, following from the above expressions, are the topic of the next section.

V. TRANSMISSION SPECTRA

In the following, we show the results for the transmission with the probe on the qubit, Eq. (20), both in the static case and in the presence of the drive on the qubit. In the latter case,

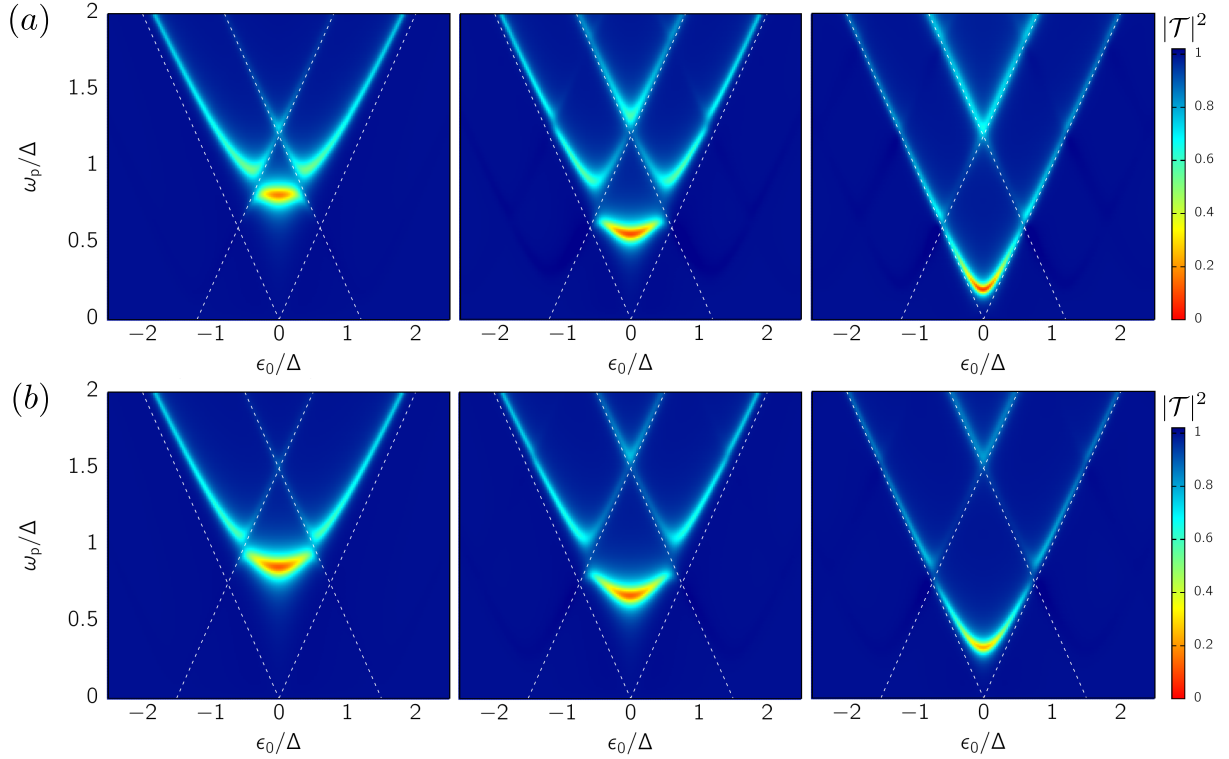


Fig. 2. Transmission spectra of the static system for two resonator frequencies: $\Omega = 1.2 \Delta$ (a) and $\Omega = 1.5 \Delta$ (b). For each panel, three values of the qubit-resonator coupling strength are considered. From left to right: $g/\Delta = 0.2, 0.5$, and 1 . Other parameters are $\kappa = 0.005$, $\alpha_1 = 0.05$ and $\omega_c = 10 \Delta$. The temperature is $k_B T = 0.1 \hbar \Delta$ for both baths. The transmission is evaluated using Eq. (20) with \mathcal{N} chosen differently for each panel in order to have the minimum of the transmission around zero. The dashes lines are at $\omega_p = \pm \epsilon_0 + l\Omega$.

we fix the drive frequency to the value $\omega_d = 2.7 \Delta$. In order to see how the picture of the static, dissipative Rabi model is impacted by a classical drive on the qubit, we start by showing in Fig. 2 the static case for two resonator frequencies, $\Omega/\Delta = 1.2, 1.5$. For both settings, we consider three values of the qubit-resonator coupling, namely $g/\Delta = 0.2, 0.5$ and 1 , the latter two being well into the USC regime. The picture that emerges from the spectra is drastically different with respect to standard spectroscopy of USC systems, where the transmission is recorded by probing the resonator [13]. In our transmission measurement protocol, which essentially measures the qubit operator σ_z , the transmission is given by the difference in populations of the

states $|\uparrow\rangle, |\downarrow\rangle$ of the qubit basis. As such, the resonator is traced out from the dynamical response of the system and its presence is reflected in the pattern of resonances involving qubit and resonator. Qualitatively, this leads to a spectrum resembling the one of the qubit alone, with a principal feature, a pronounced dip centered at $\epsilon_0 = 0$ which, for $|\epsilon_0| < \Omega$, is faithfully reproduced by the transition frequency $\tilde{\omega}_{10}$ (see below) between the first excited and the ground state of the Rabi model, renormalized by the Ohmic bath acting on the qubit ($\nu = 1$).

There are, however, two major modifications that are peculiar of the Rabi model. i) Emission and absorption of l oscillator quanta produce *sidebands* of the main spectral features, departing from $\epsilon_0 = \pm l\Omega$. ii) Avoided crossings appear which signal the strong resonator-qubit entanglement, according to Eqs. (7) and (8).

For our analysis, we introduce the bath-renormalized transition frequencies

$$\tilde{\omega}_{nm} = (\tilde{E}_n - \tilde{E}_m)/\hbar, \quad (24)$$

where \tilde{E}_n are the eigenenergies of the closed Rabi model calculated by substituting the bare qubit splitting Δ with its dissipation-renormalized version: $\Delta \rightarrow \Delta_T$, where $\Delta_T = \Delta_r (2\pi k_B T_1 / \hbar \Delta_r)^{\alpha_1}$ with $\Delta_r = \Delta(\Delta/\omega_c)^{[\alpha_1/(1-\alpha_1)]}$ [21].

Let us first focus on the undriven case. In the absence of the resonator, the principal dip at zero static bias occurs at $\omega_p \sim \Delta$ for weak dissipation and is renormalized downwards for increased system-bath coupling, see [25, Fig. 2]. In Fig. 2, the presence of the (dissipative) resonator introduces the crossing patterns and moves this principal feature towards lower frequencies upon increasing g , whereas the dissipation on the qubit is fixed in a weak-to-moderate regime. This effect can be understood in terms of the renormalization of Δ by Laguerre polynomials discussed in Sec. III A, see Eq. (10), which yields the spectrum of the Rabi model. Thus now $\omega_p \simeq \Delta_T \exp(-\tilde{\alpha}/2)$.

The resonances that follow the pattern of the dashed lines in Fig. 2, away from the avoided crossings, are explained in terms of the spectrum of the Rabi model at $\Delta = 0$, Eq. (6), with the energy differences given by $(E_{+,j} - E_{-,j'})/\hbar = \epsilon_0 + (j - j')\Omega$. On the other hand, the avoided crossings are dominated by the dressed tunneling element in Eq. (10), which shows a non-monotonic behavior with respect to g , at nonzero static bias. This is reflected, in both panels of Fig. 2, by the separation between the central dip and the tails which increases from

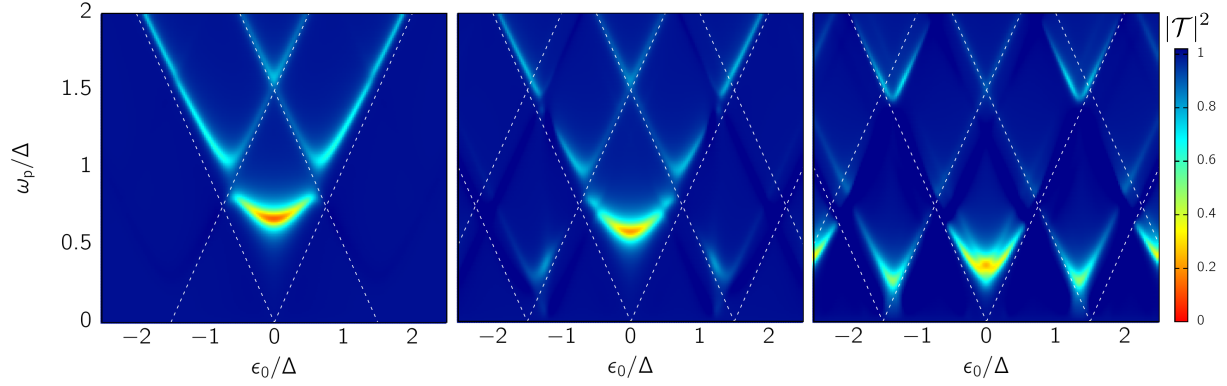


Fig. 3. Transmission spectra of the driven system for $\Omega = 1.5 \Delta$ and $g/\Delta = 0.5$. Three values of the drive amplitude are considered. From left to right: $\epsilon_d/\Delta = 0, 2$, and 4.1 . Note that the panel on the left coincides with the central panel of Fig. 2(b). The drive frequency is fixed to the value $\omega_d/\Delta = 2.7$. Other parameters are as in Fig. 2. We note that increasing the driving strength has the two-fold effect of downward-renormalizing the frequency of the principal dip at zero bias, similarly to what happens as g is increased in the static system (see Fig. 2), and of creating a pattern of multi-photon resonances for $\epsilon_0 \neq 0$.

$g = 0.2 \Delta$ to $g = 0.5 \Delta$, to shrink again upon further increasing the coupling to $g = \Delta$. E.g. the lowest avoided crossing follows the behavior of $\Delta_0^1 \simeq \Delta_T \sqrt{\tilde{\alpha}} \exp(-\tilde{\alpha}/2)$.

A similar picture is revealed by Fig. 3, where we consider the spectra in the presence of the drive, for three values of the drive amplitude, the first being $\epsilon_d = 0$ for reference. While varying the drive amplitude, we fix the coupling to $g = 0.5 \Delta$. Here, additional renormalization of Δ with appropriate Bessel functions is expected, see Eqs. (14) and (16). For the main transmission dip the zero order Bessel function is involved, and its location and dependence on the drive is well reproduced by the replacement

$$\Delta \rightarrow \Delta_T |J_0(\epsilon_d/\omega_d)|. \quad (25)$$

In the resulting set of spectra, the drive amplitude ϵ_d takes the role played by g in the static case, in that ϵ_d tunes the frequency of the main transmission dip and the size of the avoided crossings. A detailed account of this effect for zero static bias is provided in Fig. 4(b). Additional features emerge in the driven case displayed in Fig. 3 which are due to multiple resonances of

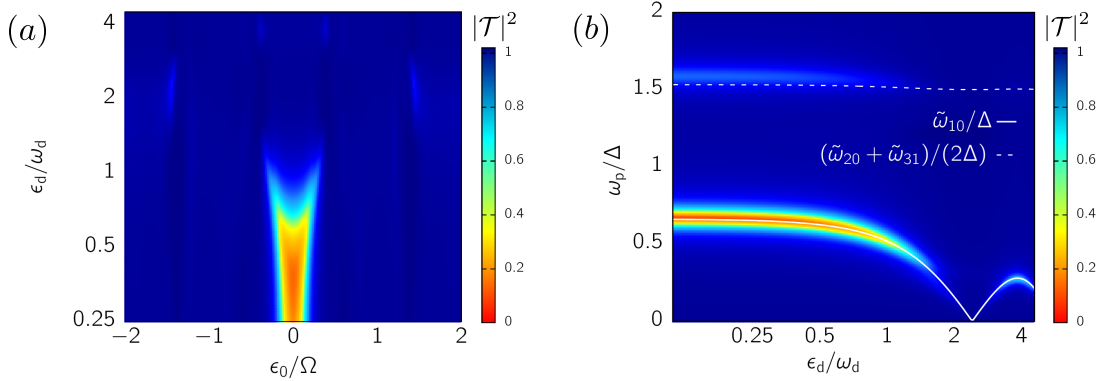


Fig. 4. Bessel pattern from drive-induced renormalization of the resonances. (a) Transmission as a function of the static bias ϵ_0 and of the drive amplitude ϵ_d , with fixed $\omega_p/\Delta = 0.65$. (b) Transmission spectrum, as a function of the drive amplitude, for $\epsilon_0 = 0$. For both panels, the other parameters are as in Fig. 3. The solid and dashed curves in panel (b) are given by the renormalized transition frequencies $\tilde{\omega}_{ij}$, Eqs. (24)-(25). Note that, as the spectrum of the Rabi model forms energy doublets, the qubit spectroscopy resolves the ground-first excited state and also the inter-doublet transitions. In the transition frequency $\tilde{\omega}_{10}$ it is clearly visible the Bessel pattern induced by the function $J_0(\epsilon_d/\omega_d)$ due to the drive.

the bias with the drive frequency, see Eqs. (13) and (14). These resonances yield replicas of the Rabi pattern, in the form of sidebands, centered at the values of static bias matching multiples of the resonator frequency. An interesting feature emerging by comparison of the central and the right panels of Fig. 3 is that, while the central pattern fades for increased drive amplitude, the side replicas are enhanced. This is due to the fact that, depending on the bias, the dressed tunneling element is modulated by Bessel functions $J_n(x)$ with different index n . In the case of Fig. 3, the central pattern, $\epsilon_0 \sim 0$ is modulated by $J_0(\epsilon_d/\omega_d)$ and the side replicas by $J_1(\epsilon_d/\omega_d)$.

This Bessel pattern is highlighted in Fig. 4. In panel (a), the qubit transmission in the driven case is shown as a function of the static bias and of the drive amplitude, displaying the "v"-shaped trace centered at zero bias. The modulation by $J_0(\epsilon_d/\omega_d)$ causes the suppression of the qubit response at zero bias when the first zero of J_0 is reached. The plot shows the system's response at a specific probe frequency ω_p . By setting the static bias to zero, we study in Fig. 4(b) the full spectrum *vs.* the drive amplitude. Such spectrum reveals that the renormalized transition

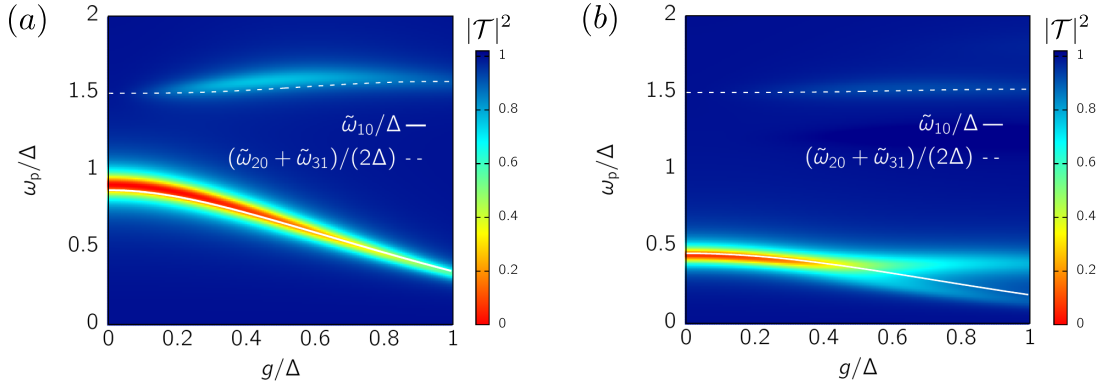


Fig. 5. Laguerre renormalization at $\epsilon_0 = 0$. (a) Transmission at zero bias *vs.* the qubit-resonator coupling g and the probe frequency ω_p in the static case, $\epsilon_d = 0$. (b) Driven case with $\epsilon_d = 4 \Delta$. For both panels the other parameters are as in Fig. 3. The solid and dashed curves are given by the renormalized transition frequencies $\tilde{\omega}_{ij}$, see Eq. (24), where $\tilde{\Delta} = \Delta_T$ in the static case (a) and $\tilde{\Delta} = \Delta_T |J_0(\epsilon_d/\omega_d)|$ in the driven case (b). Panel (a) displays, in the transition $\tilde{\omega}_{10}$, the Laguerre pattern from L_0 whereas, in panel (b), the splitting of the resonance is given by higher order Laguerre polynomials stemming from the interplay of the resonator with the drive [34].

frequency $\tilde{\omega}_{10}$ follows the Bessel pattern induced by $J_0(\epsilon_d/\omega_d)$ as suggested by Eq. (16). For this reason, in the presence of the drive, the renormalized transition frequencies in Eq. (24) are calculated from Eqs (24) and (25). The higher-frequency features in the spectrum of Fig. 4(b) are not resolved individually due to dissipation and are therefore reproduced by the (renormalized) inter-doublet transition energy $(\tilde{E}_3 - \tilde{E}_2)/2 - (\tilde{E}_1 - \tilde{E}_0)/2$.

The same is true for both panels of Fig. 5, where we show the spectrum at zero static bias as a function of the qubit-resonator coupling strength, for $\epsilon_d = 0$ and $\epsilon_d = 4 \Delta$. In panel (a), the features in the transmission are reproduced by the transition frequencies in Eq. (24) calculated with $\Delta \rightarrow \Delta_T$. Panel (b) of Fig. 5 shows that the condition that $l = 0$ at zero bias, $\epsilon_0 = 0$, used for the spectrum of the static system is no more generally true. Indeed, as can be seen from Eq. (14), the drive introduces novel resonance conditions with $l \neq 0$, i.e. when $l\Omega = m\omega_d$. In turn, this allows the contribution of dressed tunneling elements of the type $\Delta_{n,j}^{n+m,j+l}$. If $j = 1$ and $l = 1$, this involves the Laguerre polynomial $L_1^1(\tilde{\alpha})$, which has a nonmonotonic behavior with respect to $\tilde{\alpha} = (2g/\Omega)^2$. The combined effect of the different resonances in the presence of

the driving at $\epsilon_0 = 0$ is the splitting of the main resonance in Fig. 5(b), a feature which is not visible in the absence of driving, Fig. 5(a), as $l = 0$ and the dressed tunneling element in Eq. (8) is Δ_j^j , which is modulated by $L_0^0(\tilde{\alpha})$, yielding a simple exponential suppression. Note that the simple replacement in Eq. (25) in the spectrum of the Rabi model is not able to capture this multi-photon feature.

VI. CONCLUSIONS

In summary, we have theoretically investigated transmission spectra of the driven Rabi model in the USC regime. Recent experiments by Yoshihara et al. [13] have provided spectroscopic data of the (undriven) Rabi model in the deep USC regime, with the probe signal being coupled to the cavity resonator. In the set-up considered in this work, in contrast, the probe couples to the qubit. Hence, the relevant observable is the population difference between the qubit's supercurrent states. This in turn implies a different spectral response than so far reported in the literature [13, 14]. Nevertheless, also in our simulations the entangled nature of the UCS states is clearly revealed. As a future development, a similar analysis could be carried out considering the probe applied via the transmission line coupled to the resonator, which is already included in the experimental setup considered here.

When probing the qubit, the strong coupling to the quantized resonator leads to sidebands in the spectrum, reflecting multiple absorption or emission of cavity quanta. Furthermore, the doublet structure of the Rabi system is reflected in avoided crossings between subbands. In the absence of the drive, the lowest avoided crossing first increases and then decreases as a function of the coupling strength, in a characteristic way expected from displaced oscillator states. When also the drive is present, additional photon sidebands appear which also display avoided crossings. An advantage of this set-up is the possibility to tune the light-matter coupling in a continuous way. Indeed, the size and position of the avoided crossings depend on both the driving parameters as well as on the qubit-resonator coupling strength. A characteristic Bessel/Laguerre evolution as a function of the driving/coupling strength confirms the strong entanglement of the qubit with both displaced photons of the drive as well as of the resonator.

In summary, we presented theoretical predictions for the transmission spectra of the driven

dissipative Rabi model. Our results provide new insight and tools to investigate the physics of USC systems. Furthermore, they can be used to optimize the design of future experiments and for the interpretation of spectroscopic spectra.

VII. ACKNOWLEDGMENTS

L. M. and M. G. acknowledge support by the BMBF (German Ministry for Education and Research), project 13N15208, QuantERA SiUCs. P. F.-D. acknowledges support from "la Caixa" Foundation - Junior leader fellowship (ID100010434-LCF/BQ/PR19/11700009), Ministry of Science and Innovation and Agencia Estatal de Investigación (FIS2017-89860-P; SEV-2016-0588; PCI2019-111838-2), European Commission (FET-Open AVaQus GA 899561; QuantERA SiUCs), and program "Doctorat Industrial" of the Agency for Management of University and Research Grants (2020 DI 41; 2020 DI 42). IFAE is partially funded by the CERCA program of the Generalitat de Catalunya.

Appendix A: Sepctral density functions and effective structured bath

The Caldeira-Leggett model describes an open system bi-linearly interacting via the operator \hat{X} with a heat bath of harmonic oscillators

$$H_{\text{CL}} = \frac{\hat{P}^2}{2M} + V(\hat{X}) + \frac{1}{2} \sum_{j=1}^N \left[\frac{\hat{p}_j^2}{m_j} + m_j \omega_j^2 \left(\hat{x}_j - \frac{c_j}{m_j \omega_j^2} \hat{X} \right)^2 \right]. \quad (\text{A1})$$

The interaction term is $\hat{X} \sum_j c_j \hat{x}_j$ and the spectral density function $J(\omega)$ is defined as

$$J(\omega) = \frac{\pi}{2} \sum_{j=1}^N \frac{c_j^2}{m_j \omega_j} \delta(\omega - \omega_j). \quad (\text{A2})$$

For a bosonic bath we have $\hat{x}_j = \sqrt{\hbar/2m_j\omega_j}(a_j + a_j^\dagger)$. Introducing the dimensionless system position operator $\hat{Q} := \hat{X}/X_0$ we can write

$$H_{\text{CL}} = H_{\text{S}} + \sum_l \hbar \omega_j a_j^\dagger a_j - \hat{Q} \sum_j \hbar \lambda_j (a_j + a_j^\dagger) + A^2, \quad (\text{A3})$$

where A^2 is proportional to the square of \hat{X} . If the open system is a qubit, this term is a constant since $\sigma_z^2 = \mathbf{1}$ while for a harmonic oscillator it constitutes a nonlinear term which ensures

position-independent friction [21]. In Eq. (A3), we introduced the coupling with dimension of an angular frequency

$$\lambda_j = \frac{X_0}{\sqrt{2\hbar m_j \omega_j}} c_j .$$

In the context of the spin-boson model, it is also customary to define the modified spectral density function

$$G(\omega) := \sum_{j=1}^N \lambda_j^2 \delta(\omega - \omega_j) = \frac{X_0^2}{\pi \hbar} J(\omega) . \quad (\text{A4})$$

For an Ohmic bath, in the continuum limit, $J(\omega) = M\gamma\omega$.

- If the system coupled to the bath is a harmonic oscillator then $\hat{X} = X_0(B^\dagger + B)$, with $X_0 = \sqrt{\hbar/2M\Omega}$. Setting $G(\omega) = \kappa\omega$, Eq. (A4) yields $\kappa = M\gamma X_0^2/(\pi/\hbar)$ and we can identify $\gamma = 2\pi\kappa\Omega$.
- For a qubit coupled to the Ohmic bath the coupling coordinate is $\hat{X} = (X_0/2)\sigma_z$, where X_0 is the interwell distance [21]. The SB spectral density function is defined as $G(\omega) = 2\alpha\omega$. From Eq. (A4) we have $\alpha = M\gamma X_0^2/(2\pi/\hbar)$.

Appendix B: The driven, dissipative Rabi model within NIBA

As shown in Sec. IV, the transmission is related to the response of the qubit to the probe field via the population difference $P(t)$, i.e. the expectation value of σ_z , expressed in the localized (flux) states of the qubit. An exact formal expression for $P(t)$ in the presence of external heat baths, the Ohmic bath and the dissipative resonator in our case, and of a classical time-dependent drive can be given within the path integral representation of the qubit reduced dynamics [69, 70].

Within the non-interacting blip approximation (NIBA) [20, 67] of the exact path integral expression, the time evolution of the population difference can be given in terms of a generalized master equation (GME) which is nonperturbative in the qubit-baths coupling [21, 37, 71] and reads

$$\dot{P}(t) = \int_{t_0}^t dt' [K^-(t, t') - K^+(t, t')P(t')] . \quad (\text{B1})$$

The NIBA has been applied in the presence of multiple baths, notably in the context of heat transport, see e.g. [72–74]. Numerical approaches that target structured baths are discussed in [75]. In the presence of the time-dependent bias in Eq. (2), the kernels of the GME (B1), within NIBA, read [37]

$$\begin{aligned} K^+(t, t') &= h^+(t - t') \cos [\zeta_{\text{full}}(t, t')] , \\ K^-(t, t') &= h^-(t - t') \sin [\zeta_{\text{full}}(t, t')] , \end{aligned} \quad (\text{B2})$$

with the dynamical phase reading

$$\begin{aligned} \zeta_{\text{full}}(t, t') &= \int_{t'}^t dt'' \epsilon(t'') \\ &= \epsilon_0(t - t') + \frac{\epsilon_{\text{p}}}{\omega_{\text{p}}} [\sin(\omega_{\text{p}}t) - \sin(\omega_{\text{p}}t')] + \frac{\epsilon_{\text{d}}}{\omega_{\text{d}}} [\sin(\omega_{\text{d}}t) - \sin(\omega_{\text{d}}t')] , \end{aligned} \quad (\text{B3})$$

and where

$$\begin{aligned} h^+(t) &= \Delta^2 e^{-Q'(t)} \cos[Q''(t)] , \\ h^-(t) &= \Delta^2 e^{-Q'(t)} \sin[Q''(t)] . \end{aligned} \quad (\text{B4})$$

The baths correlation function $Q(t)$ is the sum of the contributions from the different baths, $Q(t) = \sum_{\nu} Q_{\nu}(t)$ [Segal2011]. In our model, $Q(t) = Q_1(t) + Q_2(t)$, where the contribution from the Ohmic bath with exponential cutoff, acting directly on the qubit ($\nu = 1$) is, in the so-called scaling limit [21],

$$Q'_1(t) = 2\alpha_1 \ln \left[\sqrt{1 + \omega_c^2 t^2} \frac{\sinh[\pi t / (\hbar\beta_1)]}{\pi t / (\hbar\beta_1)} \right] , \quad (\text{B5})$$

$$Q''_1(t) = 2\alpha_1 \arctan(\omega_c t) . \quad (\text{B6})$$

Applying Eq. (23) to the spectral density function $G_2(\omega)$ one obtains for the effective bath of the dissipative resonator ($\nu = 2$) [55, 56, 62]

$$Q'_2(t) = Xt + L \left(e^{-\gamma t/2} \cos \bar{\Omega}t - 1 \right) - Ze^{-\gamma t/2} \sin \bar{\Omega}t + Q'_{\text{Mats}}(t) , \quad (\text{B7})$$

$$Q''_2(t) = \pi\alpha_2 - e^{-\gamma t/2} \pi\alpha (\cos \bar{\Omega}t + N \sin \bar{\Omega}t) , \quad (\text{B8})$$

with $X = 2\pi\alpha_2 k_B T / \hbar$ and $\bar{\Omega} = \sqrt{\Omega^2 - \gamma^2/4}$ and where

$$\begin{aligned} N &= \frac{\gamma^2/2 - \Omega^2}{\gamma\bar{\Omega}} , \\ L &= \pi\alpha_2 \frac{N \sinh(\beta\hbar\bar{\Omega}) + \sin(\beta\hbar\gamma/2)}{\cosh(\beta\hbar\bar{\Omega}) - \cos(\beta\hbar\gamma/2)} , \\ Z &= \pi\alpha_2 \frac{\sinh(\beta\hbar\bar{\Omega}) - N \sin(\beta\hbar\gamma/2)}{\cosh(\beta\hbar\bar{\Omega}) - \cos(\beta\hbar\gamma/2)} . \end{aligned} \quad (\text{B9})$$

The term $Q'_{\text{Mats}}(t)$ is the following series over the Matsubara frequencies $\nu_n := n \, 2\pi k_B T / \hbar$

$$Q'_{\text{Mats}}(t) = 4\pi\alpha_2 \frac{\Omega^4}{\hbar\beta} \sum_{n=1}^{+\infty} \frac{1}{(\Omega^2 + \nu_n^2)^2 - \gamma^2 \nu_n^2} \left[\frac{1 - e^{-\nu_n t}}{\nu_n} \right] . \quad (\text{B10})$$

Appendix C: linear susceptibility in the presence of a high-frequency drive

Averaging the kernels in Eq. (B2) over a drive period $T_d = 2\pi/\omega_d$, we make the substitution $K^\pm(t, t') \rightarrow K_d^\pm(t, t')$ in the GME, where

$$\begin{aligned} K_d^+(t, t') &= h_d^+(t - t') \cos[\zeta(t, t')] , \\ K_d^-(t, t') &= h_d^-(t - t') \sin[\zeta(t, t')] , \end{aligned} \quad (\text{C1})$$

with the dynamical phase $\zeta(t, t')$ which is now independent of the drive, as it contains exclusively the static bias and the time-dependent probe

$$\zeta(t, t') = \epsilon_0(t - t') + \frac{\epsilon_p}{\omega_p} [\sin(\omega_p t) - \sin(\omega_p t')] , \quad (\text{C2})$$

cf. Eq. (B3). The drive is taken into account effectively by the functions

$$\begin{aligned} h_d^+(t) &= \Delta^2 e^{-Q'(t)} \cos[Q''(t)] J_0 \left[\frac{2\epsilon_d}{\omega_d} \sin\left(\frac{\omega_d t}{2}\right) \right] , \\ h_d^-(t) &= \Delta^2 e^{-Q'(t)} \sin[Q''(t)] J_0 \left[\frac{2\epsilon_d}{\omega_d} \sin\left(\frac{\omega_d t}{2}\right) \right] . \end{aligned} \quad (\text{C3})$$

The Bessel function can be expanded in Fourier series as

$$J_0 \left[\frac{2\epsilon_d}{\omega_d} \sin\left(\frac{\omega_d t}{2}\right) \right] = \sum_n J_n^2(\epsilon_d/\omega_d) e^{-in\omega_d t} . \quad (\text{C4})$$

Due to the effect of the monochromatic probe, we assume the asymptotic population $P_{\text{as}}(t)$ to be periodic with the period of the probe. The latter is the solution of the GME for $t_0 \rightarrow -\infty$,

namely

$$\begin{aligned}\dot{P}_{\text{as}}(t) &= \int_{-\infty}^t dt' [K_{\text{d}}^-(t, t') - K_{\text{d}}^+(t, t') P_{\text{as}}(t')] \\ &= \int_0^{\infty} d\tau [K_{\text{d}}^-(t, t - \tau) - K_{\text{d}}^+(t, t - \tau) P_{\text{as}}(t - \tau)] .\end{aligned}\tag{C5}$$

The NIBA kernels are periodical in t with the periodicity of the probe, and can be expanded in Fourier series as

$$K_{\text{d}}^{\pm}(t, t - \tau) = \sum_m k_m^{\pm}(\tau) e^{-i\omega_{\text{p}} t} ,\tag{C6}$$

where

$$k_m^{\pm}(\tau) = \frac{\omega_{\text{p}}}{2\pi} \int_{-\pi/\omega_{\text{p}}}^{\pi/\omega_{\text{p}}} dt K_{\text{d}}^{\pm}(t, t - \tau) e^{im\omega_{\text{p}} t} .\tag{C7}$$

Defining $c^+(x) = \cos(x)$ and $c^-(x) = \sin(x)$, from Appendix D, we can write for $m = 0, 1$

$$\begin{aligned}k_0^{\pm}(\tau) &= h_{\text{d}}^{\pm}(\tau) c^{\pm}(\epsilon_0 \tau) , \\ k_1^{\pm}(\tau) &= \mp \frac{\epsilon_{\text{p}}}{\omega_{\text{p}}} e^{i\omega_{\text{p}} \tau / 2} h_{\text{d}}^{\pm}(\tau) \sin(\omega_{\text{p}} \tau / 2) c^{\mp}(\epsilon_0 \tau) ,\end{aligned}\tag{C8}$$

which are of order 0 and 1, respectively, in the ratio $\epsilon_{\text{p}}/\omega_{\text{p}}$.

Under the assumption that the memory time of the kernels is finite, $t_{\text{memory}} < \infty$, so that when the kernels are different from zero the asymptotic population different is already at the steady state, $P(t) = P_{\text{as}}(t)$, we Fourier-expand $P_{\text{as}}(t)$ on the LHS and inside the integral in the GME (C5). The latter adopts the form

$$\sum_m -im\omega_{\text{p}} p_m e^{-im\omega_{\text{p}} t} = \int_0^{\infty} d\tau \sum_m k_m^-(\tau) e^{-im\omega_{\text{p}} t} - \int_0^{\infty} d\tau \sum_{m,n} k_m^+(\tau) e^{-i(m+n)\omega_{\text{p}} t} p_n e^{in\omega_{\text{p}} \tau} .$$

Defining

$$\hat{k}_m^{\pm}(\lambda) = \int_0^{\infty} d\tau e^{-\lambda \tau} k_m^{\pm}(\tau) ,\tag{C9}$$

Eq. (C9) reads

$$\sum_m -im\omega_{\text{p}} p_m e^{-im\omega_{\text{p}} t} = \sum_m \hat{k}_m^-(0) e^{-im\omega_{\text{p}} t} - \sum_{m,n} \hat{k}_m^+(-in\omega_{\text{p}}) p_n e^{-i(m+n)\omega_{\text{p}} t}\tag{C10}$$

Taking the component at frequency ω_p

$$-i\omega_p p_1 = \hat{k}_{+1}^-(0) - \sum_{m+n=1} \hat{k}_m^+(-in\omega_p) p_n \quad (\text{C11})$$

Since $\hat{k}_m(\lambda) \propto (\epsilon_p/\omega_p)^{|m|}$, see Eq. (C8), we have

$$p_1(\omega_p) = \frac{1}{-i\omega_p + \hat{k}_0^+(-i\omega_p)} \left[\hat{k}_{+1}^-(0) - \hat{k}_{+1}^+(0) p_0 \right] + \mathcal{O}[(\epsilon_p/\omega_p)^2] . \quad (\text{C12})$$

Taking the zero-frequency component of Eq. (C9)

$$0 = \hat{k}_0^-(0) - \hat{k}_0^+(0) p_0 + \mathcal{O}(\epsilon_p/\omega_p) .$$

Thus, to the lowest order in the probe amplitude [37, 75]

$$p_1(\omega_p) = \frac{1}{-i\omega_p + \hat{k}_0^+(-i\omega_p)} \left[\hat{k}_{+1}^-(0) - \hat{k}_{+1}^+(0) \frac{\hat{k}_0^-(0)}{\hat{k}_0^+(0)} \right] , \quad (\text{C13})$$

where, from Eqs. (C8) and (C9),

$$\begin{aligned} \hat{k}_0^\pm(\lambda) &= \int_0^\infty d\tau e^{-\lambda\tau} h_d^\pm(\tau) c^\pm(\epsilon_0\tau) \\ \hat{k}_1^\pm(0) &= \mp \frac{\epsilon_p}{\omega_p} \int_0^\infty d\tau e^{i\omega_p\tau/2} h_d^\pm(\tau) \sin(\omega_p\tau/2) c^\mp(\epsilon_0\tau) . \end{aligned} \quad (\text{C14})$$

The corresponding expression for the linear susceptibility $\chi(\omega_p) = p_1(\omega_p)/\hbar\epsilon_p$ is given in Eq. (21). This expression is the one used throughout the present work.

Markovian limit

For completeness we also give the susceptibility in the Markovian limit, namely when the decay time of the kernels is much shorter than the relevant time scales of variation of $P(t)$. In this case

$$\dot{P}_{\text{as}}(t) = \int_0^\infty d\tau K_d^-(t, -\tau) - \int_0^\infty d\tau K_d^+(t, t - \tau) P_{\text{as}}(t) . \quad (\text{C15})$$

By expanding the kernels in Fourier series we obtain the equation

$$\sum_m -im\omega_p p_m e^{-im\omega_p t} = \sum_m \hat{k}_m^-(0) e^{-im\omega_p t} - \sum_{m,n} \hat{k}_m^+(0) p_n e^{-i(m+n)\omega_p t} \quad (\text{C16})$$

whose component at frequency ω_p is now

$$\begin{aligned} -i\omega_p p_1 &= \hat{k}_{+1}^-(0) - \sum_{m+n=1} \hat{k}_m^+(0) p_n e^{-i(m+n)\omega_p t} \\ &\simeq \hat{k}_{+1}^-(0) - \hat{k}_{+1}^+(0) p_0 - \hat{k}_0^+(0) p_{+1} - \hat{k}_{+2}^+(0) p_{-1} . \end{aligned} \quad (\text{C17})$$

As a result, in the Markovian limit and to the lowest order in ϵ_p/ω_p , we have

$$p_1(\omega_p) = \frac{1}{-i\omega_p + \hat{k}_0^+(0)} \left[\hat{k}_{+1}^-(0) - \hat{k}_{+1}^+(0) \frac{\hat{k}_0^-(0)}{\hat{k}_0^+(0)} \right] . \quad (\text{C18})$$

Appendix D: Calculation of $k_m^\pm(\tau)$

Using the notation $c^+(x) := \cos(x)$ and $c^-(x) := \sin(x)$, we express the dynamical phase in Eq. (C2) as

$$\begin{aligned} \zeta(t, t - \tau) &= \epsilon_0 \tau + \frac{\epsilon_p}{\omega_p} \{ \sin(\omega_p t) - \sin[\omega_p(t - \tau)] \} \\ &= \epsilon_0 \tau + 2 \frac{\epsilon_p}{\omega_p} \cos(\omega_p t - \phi_\tau) \sin(\phi_\tau) \\ &= \epsilon_0 \tau + E(t, \tau) , \end{aligned} \quad (\text{D1})$$

where $\phi_\tau := \omega_p \tau / 2$. As a result

$$c^\pm[\zeta(t, t - \tau)] = c^\pm(\epsilon_0 \tau) c^\pm[E(t, \tau)] \mp c^\mp(\epsilon_0 \tau) c^\mp[E(t, \tau)] \quad (\text{D2})$$

From Eq. (C1)

$$\begin{aligned} k_m^\pm(\tau) &= \frac{\omega_p}{2\pi} \int_{-\pi/\omega_p}^{\pi/\omega_p} dt K_d^\pm(t, t - \tau) e^{im\omega_p t} \\ &= h_d^\pm(\tau) \frac{\omega_p}{2\pi} \int_{-\pi/\omega_p}^{\pi/\omega_p} dt c^\pm[\zeta(t, t - \tau)] e^{im\omega_p t} \\ &= h_d^\pm(\tau) [c^\pm(\epsilon_0 \tau) F_m^+(\tau) \mp c^\mp(\epsilon_0 \tau) F_m^-(\tau)] , \end{aligned} \quad (\text{D3})$$

where

$$\begin{aligned} F_m^\pm(\tau) &= \frac{\omega_p}{2\pi} \int_{-\pi/\omega_p}^{\pi/\omega_p} dt e^{im\omega_p t} c^\pm[E(t, \tau)] \\ &= \frac{e^{im\phi_\tau}}{2\pi} \int_{-\pi-\phi_\tau}^{\pi-\phi_\tau} dx c^\pm \left[\frac{2\epsilon_p}{\omega_p} \cos(x) \sin(\phi_\tau) \right] e^{imx} \\ &= \frac{e^{im\phi_\tau}}{2\pi} \int_{-\pi}^{\pi} dx c^\pm [z \cos(x)] e^{imx} , \end{aligned} \quad (\text{D4})$$

with $x := \omega_p t - \phi_\tau$ and $z := 2\epsilon_p \sin(\phi_\tau)/\omega_p$. In the last line we have shifted the integration domain (of length one period) exploiting the periodicity of the integrand. Since only the even part of the integrand contributes to the integral in Eq. (D4), we can write the latter as [68]

$$\begin{aligned} F_m^\pm(\tau) &= \frac{e^{im\phi_\tau}}{\pi} \int_0^\pi dx \, c^\pm [z \cos(x)] i^{(1\mp 1)/2} c^\pm(mx) \\ &= \frac{e^{im\phi_\tau}}{2\pi} \int_0^\pi dx \, \left[e^{iz \cos(x)} \pm e^{-iz \cos(x)} \right] c^\pm(mx) \\ &= e^{im\phi_\tau} i^{m-(1\mp 1)/2} \frac{J_m(z) \pm J_m(-z)}{2}, \end{aligned} \quad (\text{D5})$$

where J_m is the Bessel function of order m which has the parity $J_m(-z) = (-1)^m J_m(z)$. As a result

$$F_m^+(\tau) = \begin{cases} i^m e^{im\omega_p \tau/2} J_m \left[\frac{2\epsilon_p}{\omega_p} \sin \left(\frac{\omega_p \tau}{2} \right) \right], & m \text{ even} \\ 0, & m \text{ odd} \end{cases} \quad (\text{D6})$$

and

$$F_m^-(\tau) = \begin{cases} 0, & m \text{ even} \\ i^{m-1} e^{im\omega_p \tau/2} J_m \left[\frac{2\epsilon_p}{\omega_p} \sin \left(\frac{\omega_p \tau}{2} \right) \right], & m \text{ odd} \end{cases}. \quad (\text{D7})$$

To lowest order in z we have $J_m(z) \simeq (z/2)^m$. Then, substituting the above expressions for $F_m^\pm(\tau)$ into Eq. (D3), we obtain

$$k_m^\pm(\tau) \simeq h_d^\pm(\tau) \begin{cases} i^m e^{im\omega_p \tau/2} \left[\frac{\epsilon_p}{\omega_p} \sin \left(\frac{\omega_p \tau}{2} \right) \right]^m c^\pm(\epsilon_0 \tau), & m \text{ even} \\ \mp i^{m-1} e^{im\omega_p \tau/2} \left[\frac{\epsilon_p}{\omega_p} \sin \left(\frac{\omega_p \tau}{2} \right) \right]^m c^\mp(\epsilon_0 \tau), & m \text{ odd} \end{cases}, \quad (\text{D8})$$

to lowest order in ϵ_p/ω_p .

References

- [1] J. Q. You and F. Nori, “Atomic physics and quantum optics using superconducting circuits,” [Nature](#) **474**, 589–597 (2011).
- [2] A. A. Houck, H. E. Türeci, and J. Koch, “On-chip quantum simulation with superconducting circuits,” [Nat. Phys.](#) **8**, 292 (2012).

- [3] J. P. Pekola, “Towards quantum thermodynamics in electronic circuits,” [Nat. Phys. **11**, 118–123 \(2015\).](#)
- [4] G. Wendin, “Quantum information processing with superconducting circuits: a review,” [Rep. Prog. Phys. **80**, 106001 \(2017\).](#)
- [5] X. Gu, A. F. Kockum, A. Miranowicz, Y.-X. Liu, and F. Nori, “Microwave photonics with superconducting quantum circuits,” [Phys. Rep. **718–719**, 1–102 \(2017\).](#)
- [6] C. Ciuti, G. Bastard, and I. Carusotto, “Quantum vacuum properties of the intersubband cavity polariton field,” [Phys. Rev. B **72**, 115303 \(2005\).](#)
- [7] J. Bourassa, J. M. Gambetta, A. A. Abdumalikov, O. Astafiev, Y. Nakamura, and Blais A., “Ultrastrong coupling regime of cavity QED with phase-biased flux qubits,” [Phys. Rev. A **80**, 032109 \(2009\).](#)
- [8] J. Hausinger and M. Grifoni, “Dissipative dynamics of a biased qubit coupled to a harmonic oscillator: analytical results beyond the rotating wave approximation,” [New J. Phys. **10**, 115015 \(2008\).](#)
- [9] T. Niemczyk *et al.*, “Circuit quantum electrodynamics in the ultrastrong-coupling regime,” [Nat. Phys. **6**, 772–776 \(2010\).](#)
- [10] S. Ashhab and F. Nori, “Qubit-oscillator systems in the ultrastrong-coupling regime and their potential for preparing nonclassical states,” [Phys. Rev. A **81**, 042311 \(2010\).](#)
- [11] J. Hausinger and M. Grifoni, “Qubit-oscillator system: An analytical treatment of the ultrastrong coupling regime,” [Phys. Rev. A **82**, 062320 \(2010\).](#)
- [12] P. Forn-Díaz, J. Lisenfeld, D. Marcos, J. J. García-Ripoll, E. Solano, C. J. P. M. Harmans, and J. E. Mooij, “Observation of the Bloch-Siegert Shift in a Qubit-Oscillator System in the Ultrastrong Coupling Regime,” [Phys. Rev. Lett. **105**, 237001 \(2010\).](#)
- [13] F. Yoshihara, T. Fuse, S. Ashhab, K. Kakuyanagi, S. Saito, and K. Semba, “Superconducting qubit-oscillator circuit beyond the ultrastrong-coupling regime,” [Nat. Phys. **13**, 44 \(2016\).](#)
- [14] F. Yoshihara, T. Fuse, S. Ashhab, K. Kakuyanagi, S. Saito, and K. Semba, “Characteristic spectra of circuit quantum electrodynamics systems from the ultrastrong- to the deep-strong-coupling regime,” [Phys. Rev. A **95**, 053824 \(2017\).](#)
- [15] P. Forn-Díaz, L. Lamata, E. Rico, J. Kono, and E. Solano, “Ultrastrong coupling regimes of light-matter interaction,” [Rev. Mod. Phys. **91**, 025005 \(2019\).](#)
- [16] F. A. Kockum, A. Miranowicz, S. De Liberato, S. Savasta, and F. Nori, “Ultrastrong coupling between light and matter,” [Nat. Rev. Phys. **1**, 19–40 \(2019\).](#)
- [17] G. Romero, D. Ballester, Y. M. Wang, V. Scarani, and E. Solano, “Ultrafast Quantum Gates in Circuit QED,” [Phys. Rev. Lett. **108**, 120501 \(2012\).](#)

- [18] M.H. Devoret and J.M. Martinis, “Implementing qubits with superconducting integrated circuits,” *Quantum Inf. Process.* **3**, 163–203 (2004).
- [19] J. E. Mooij, T. P. Orlando, L. Levitov, L. Tian, C. H. van der Wal, and S. Lloyd, “Josephson Persistent-Current Qubit,” *Science* **285**, 1036 (1999).
- [20] A. J. Leggett, S. Chakravarty, A. T. Dorsey, M. P. A. Fisher, A. Garg, and W. Zwerger, “Dynamics of the dissipative two-state system,” *Rev. Mod. Phys.* **59**, 1–85 (1987).
- [21] U. Weiss, *Quantum Dissipative Systems* (World Scientific, Singapore, 2012, 4th ed.).
- [22] H. P. Breuer and F. Petruccione, *The theory of open quantum systems* (Oxford University Press, Oxford, 2002).
- [23] B. Peropadre, D. Zueco, D. Porras, and J. J. García-Ripoll, “Nonequilibrium and Nonperturbative Dynamics of Ultrastrong Coupling in Open Lines,” *Phys. Rev. Lett.* **111**, 243602 (2013).
- [24] P. Forn-Díaz, J. J. García-Ripoll, B. Peropadre, J. L. Orgiazzi, M. A. Yurtalan, R. Belyansky, C. M. Wilson, and A. Lupascu, “Ultrastrong coupling of a single artificial atom to an electromagnetic continuum in the nonperturbative regime,” *Nat. Phys.* **13**, 39–43 (2017).
- [25] L. Magazzù, P. Forn-Díaz, R. Belyansky, J.-L. Orgiazzi, M. A. Yurtalan, M. R. Otto, A. Lupascu, C. M. Wilson, and M. Grifoni, “Probing the strongly driven spin-boson model in a superconducting quantum circuit,” *Nat. Commun.* **9**, 1403 (2018).
- [26] J. Leppäkangas, J. Braumüller, M. Hauck, J.-M. Reiner, I. Schwenk, S. Zanker, L. Fritz, A. V. Ustinov, M. Weides, and M. Marthaler, “Quantum simulation of the spin-boson model with a microwave circuit,” *Phys. Rev. A* **97**, 052321 (2018).
- [27] P. M. Javier, L. Sébastien, N. Gheeraert, R. Dassonneville, L. Planat, F. Foroughi, Y. Krupko, O. Buisson, C. Naud, W. Hasch-Guichard, S. Florens, I. Snyman, and N. Roch, “A tunable Josephson platform to explore many-body quantum optics in circuit-QED,” *npj Quantum Inf.* **5**, 19 (2019).
- [28] R. Kuzmin, N. Mehta, N. Grabon, R. Mencia, and V. E. Manucharyan, “Superstrong coupling in circuit quantum electrodynamics,” *npj Quantum Inf.* **5**, 20 (2019).
- [29] D. Z. Rossatto, C. J. Villas-Bôas, M. Sanz, and E. Solano, “Spectral classification of coupling regimes in the quantum Rabi model,” *Phys. Rev. A* **96**, 013849 (2017).
- [30] G. Díaz-Camacho, A. Bermudez, and J. J. García-Ripoll, “Dynamical polaron Ansatz: A theoretical tool for the ultrastrong-coupling regime of circuit QED,” *Phys. Rev. Lett.* **93**, 043843 (2016).
- [31] F. Armata, G. Calajo, T. Jaako, M. S. Kim, and P. Rabl, “Harvesting Multiqubit Entanglement from Ultrastrong Interactions in Circuit Quantum Electrodynamics,” *Phys. Rev. Lett.* **119**, 183602 (2017).
- [32] D. De Bernardis, P. Pilar, T. Jaako, S. De Liberato, and P. Rabl, “Breakdown of gauge invariance

- in ultrastrong-coupling cavity QED,” *Phys. Rev. A* **98**, 053819 (2018).
- [33] O. Di Stefano, A. Settinieri, V. Macrì, L. Garziano, R. Stassi, S. Savasta, and F. Nori, “Resolution of gauge ambiguities in ultrastrong-coupling cavity quantum electrodynamics,” *Nat. Phys.* **15**, 803–808 (2019).
 - [34] J. Hausinger and M. Grifoni, “Qubit-oscillator system under ultrastrong coupling and extreme driving,” *Phys. Rev. A* **83**, 030301(R) (2011).
 - [35] W. D. Oliver, Y. Yu, J. C. Lee, K. K. Berggren, L. S. Levitov, and T. P. Orlando, “Mach-Zehnder Interferometry in a Strongly Driven Superconducting Qubit,” *Science* **310**, 1653 (2005).
 - [36] C. M. Wilson, T. Duty, F. Persson, M. Sandberg, G. Johansson, and P. Delsing, “Coherence Times of Dressed States of a Superconducting Qubit under Extreme Driving,” *Phys. Rev. Lett.* **98**, 257003 (2007).
 - [37] M. Grifoni and P. Hänggi, “Driven quantum tunneling,” *Phys. Rep.* **304**, 229–354 (1998).
 - [38] S. Kohler, “Dispersive Readout of Adiabatic Phases,” *Phys. Rev. Lett.* **119**, 196802 (2017).
 - [39] G. Engelhardt and C. Cao, “Dynamical Symmetries and Symmetry-Protected Selection Rules in Periodically Driven Quantum Systems,” *Phys. Rev. Lett.* **126**, 090601 (2021).
 - [40] V. Reimer, K. G. L. Pedersen, N. Tanger, M. Pletyukhov, and V. Gritsev, “Nonadiabatic effects in periodically driven dissipative open quantum systems,” *Phys. Rev. A* **97**, 043851 (2018).
 - [41] F. Yoshihara, T. Fuse, Z. Ao, S. Ashhab, K. Kakuyanagi, S. Saito, T. Aoki, K. Koshino, and K. Semba, “Inversion of Qubit Energy Levels in Qubit-Oscillator Circuits in the Deep-Strong-Coupling Regime,” *Phys. Rev. Lett.* **120**, 183601 (2018).
 - [42] O. Astafiev, A. M. Zagoskin, A. A. Abdumalikov, Y. A. Pashkin, T. Yamamoto, K. Inomata, Y. Nakamura, and J. S. Tsai, “Resonance Fluorescence of a Single Artificial Atom,” *Science* **327**, 840 (2010).
 - [43] I.-C. Hoi, C. M. Wilson, G. Johansson, T. Palomaki, B. Peropadre, and P. Delsing, “Demonstration of a Single-Photon Router in the Microwave Regime,” *Phys. Rev. Lett.* **107**, 073601 (2011).
 - [44] A. A. Abdumalikov, O. V. Astafiev, Y. A. Pashkin, Y. Nakamura, and J. S. Tsai, “Dynamics of Coherent and Incoherent Emission from an Artificial Atom in a 1D Space,” *Phys. Rev. Lett.* **107**, 043604 (2011).
 - [45] M. Haeberlein *et al.*, “Spin-boson model with an engineered reservoir in circuit quantum electrodynamics,” arXiv:1506.09114 (2015).
 - [46] P. Forn-Díaz, C. W. Warren, C. W. S. Chang, A. M. Vadiraj, and C. M. Wilson, “On-Demand Microwave Generator of Shaped Single Photons,” *Phys. Rev. Applied* **8**, 054015 (2017).
 - [47] I. Chiorescu, P. Bertet, K. Semba, Y. Nakamura, C. J. P. M. Harmans, and J. E. Mooij, “Coherent

- dynamics of a flux qubit coupled to a harmonic oscillator,” *Nature* **431**, 159–162 (2004).
- [48] M. Thorwart, E. Paladino, and M. Grifoni, “Dynamics of the spin-boson model with a structured environment,” *Chem. Phys.* **296**, 333–344 (2004).
 - [49] J. Johansson, S. Saito, T. Meno, H. Nakano, M. Ueda, K. Semba, and H. Takayanagi, “Vacuum Rabi Oscillations in a Macroscopic Superconducting Qubit *LC* Oscillator System,” *Phys. Rev. Lett.* **96**, 127006 (2006).
 - [50] A. Ronzani, B. Karimi, J. Senior, Y.-C. Chang, J. T. Peltonen, C.D. Chen, and J. P. Pekola, “Tunable photonic heat transport in a quantum heat valve,” *Nat. Phys.* **14**, 991–995 (2018).
 - [51] J. Lolli, A. Baksic, D. Nagy, V. E. Manucharyan, and C. Ciuti, “Ancillary Qubit Spectroscopy of Vacua in Cavity and Circuit Quantum Electrodynamics,” *Phys. Rev. Lett.* **114**, 183601 (2015).
 - [52] G. Falci, A. Ridolfo, P. G. Di Stefano, and E. Paladino, “Ultrastrong coupling probed by Coherent Population Transfer,” *Sci. Rep.* **9**, 9249 (2019).
 - [53] A. Ridolfo, G. Falci, F. M. D. Pellegrino, G. D. Maccarrone, and E. Paladino, “Photon pair production by STIRAP in ultrastrongly coupled matter-radiation systems,” *Eur. Phys. J. Spec. Top.* **227**, 2183 (2019).
 - [54] F. Beaudoin, J. M. Gambetta, and A. Blais, “Dissipation and ultrastrong coupling in circuit QED,” *Phys. Rev. A* **84**, 043832 (2011).
 - [55] A. Garg, J. N. Onuchic, and V. Ambegaokar, “Effect of friction on electron transfer in biomolecules,” *J. Chem. Phys.* **83**, 4491–4503 (1985).
 - [56] L. Magazzù and M. Grifoni, “Transmission spectra of an ultrastrongly coupled qubit-dissipative resonator system,” *J. Stat. Mech.* **2019**, 104002 (2019).
 - [57] S. De Liberato, D. Gerace, I. Carusotto, and C. Ciuti, “Extracavity quantum vacuum radiation from a single qubit,” *Phys. Rev. A* **80**, 053810 (2009).
 - [58] F. Beaudoin, J. M. Gambetta, and A. Blais, “Dissipation and ultrastrong coupling in circuit QED,” *Phys. Rev. A* **84**, 043832 (2011).
 - [59] A. O. Caldeira and A. J. Leggett, “Influence of Dissipation on Quantum Tunneling in Macroscopic Systems,” *Phys. Rev. Lett.* **46**, 211–214 (1981).
 - [60] A. O. Caldeira and A. J. Leggett, “Quantum tunnelling in a dissipative system,” *Ann. Phys.* **149**, 374–456 (1983).
 - [61] M. C. Goorden, M. Thorwart, and M. Grifoni, “Entanglement spectroscopy of a driven solid-state qubit and its detector,” *Phys. Rev. Lett.* **93**, 267005 (2004).
 - [62] F. Nesi, M. Grifoni, and E. Paladino, “Dynamics of a qubit coupled to a broadened harmonic mode at finite detuning,” *New J. Phys.* **9**, 316–316 (2007).

- [63] D. Zueco and J. J. García-Ripoll, “Ultrastrongly dissipative quantum Rabi model,” [Phys. Rev. A **99**, 013807 \(2019\)](#).
- [64] E. K. Irish, J. Gea-Banacloche, I. Martin, and K. C. Schwab, “Dynamics of a two-level system strongly coupled to a high-frequency quantum oscillator,” [Phys. Rev. B **72**, 195410 \(2005\)](#).
- [65] E. K. Irish, “Generalized Rotating-Wave Approximation for Arbitrarily Large Coupling,” [Phys. Rev. Lett. **99**, 173601 \(2007\)](#).
- [66] U. Vool and M. Devoret, “Introduction to quantum electromagnetic circuits,” [Int. J. Circ. Theor. Appl. **45**, 897–934 \(2017\)](#).
- [67] H. Dekker, “Noninteracting-blip approximation for a two-level system coupled to a heat bath,” [Phys. Rev. A **35**, 1436–1437 \(1987\)](#).
- [68] I. S. Gradshteyn and I. M. Ryzhik, *Table of Integrals, Series, and Products* (Academic Press, New York, 1980).
- [69] M. Carrega, P. Solinas, A. Braggio, M. Sassetti, and U. Weiss, “Functional integral approach to time-dependent heat exchange in open quantum systems: general method and applications,” [New J. Phys. **17**, 045030 \(2015\)](#).
- [70] M. Carrega, P. Solinas, M. Sassetti, and U. Weiss, “Energy Exchange in Driven Open Quantum Systems at Strong Coupling,” [Phys. Rev. Lett. **116**, 240403 \(2016\)](#).
- [71] L. Nicolin and D. Segal, “Non-equilibrium spin-boson model: Counting statistics and the heat exchange fluctuation theorem,” [J. Chem. Phys. **135**, 164106 \(2011\)](#).
- [72] N. Boudjada and D. Segal, “From Dissipative Dynamics to Studies of Heat Transfer at the Nanoscale: Analysis of the Spin-Boson Model,” [J. Phys. Chem. A **118**, 11323–11336 \(2014\)](#).
- [73] D. Segal, “Heat transfer in the spin-boson model: A comparative study in the incoherent tunneling regime,” [Phys. Rev. E **90**, 012148 \(2014\)](#).
- [74] T. Yamamoto, M. Kato, T. Kato, and K. Saito, “Heat transport via a local two-state system near thermal equilibrium,” [New J. Phys. **20**, 093014 \(2018\)](#).
- [75] M. Grifoni, M. Sassetti, P. Hänggi, and U. Weiss, “Cooperative effects in the nonlinearly driven spin-boson system,” [Phys. Rev. E **52**, 3596–3607 \(1995\)](#).